AD-A114 580 WISCONSIN UNIV-MADISON MATHEMATICS RESEARCH CENTER F/G 7/3
COLLOCATION ANALYSIS OF MULTICOMPONENT DIFFUSION AND REACTIONS --ETC(U)
FEB 82 J P SORENSEN, W E STEWART DAAG29-80-C-0041
UNCLASSIFIED MRC-TSR-2341 NL

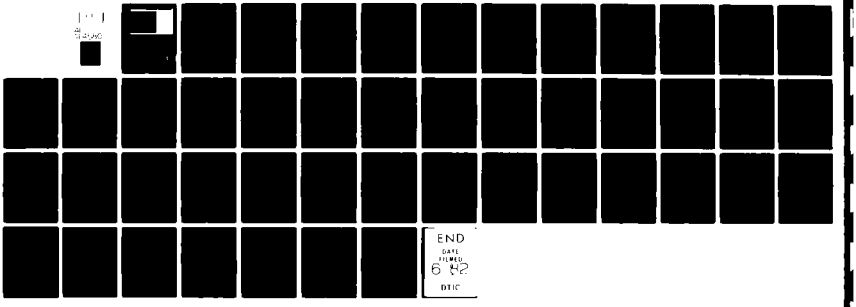

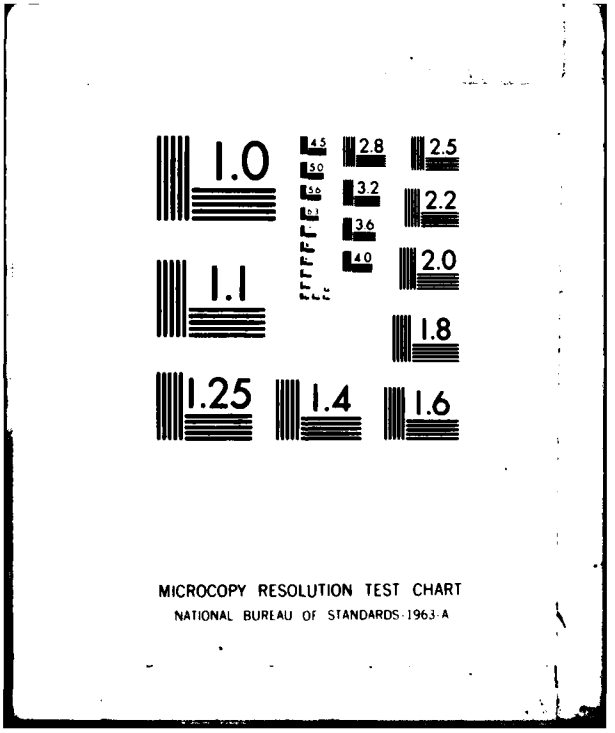
1.0
1.1
1.25
1.4
1.6
1.8
2.0
2.2
2.5
2.8
3.2
3.6
4.0
4.5
5.0
5.6
MICROCOPY RESOLUTION TEST CHART
NATIONAL BUREAU OF STANDARDS-1963-A

MRC Technical Summary Report #2341

COLLOCATION ANALYSIS OF MULTICOMPONENT DIFFUSION AND REACTIONS IN POROUS CATALYSTS

Jan P. Sørensen and Warren E. Stewart

Mathematics Research Center
University of Wisconsin—Madison
610 Walnut Street
Madison, Wisconsin 53706

February 1982

(Received November 20, 1981)

Sponsored by

U. S. Army Research Office
P. O. Box 12211
Research Triangle Park
North Carolina 27709

UNIVERSITY OF WISCONSIN - MADISON
MATHEMATICS RESEARCH CENTER

COLLOCATION ANALYSIS OF MULTICOMPONENT DIFFUSION AND REACTIONS IN POROUS CATALYSTS

Jan P. Sørensen and Warren E. Stewart*

Technical Summary Report #2341
February 1982

ABSTRACT

A collocation method is given for steady-state simulation of multiple reactions in porous catalysts. A realistic multicomponent diffusion model is used, which includes an allowance for pore size distribution. Hyperbolic basis functions are introduced to represent the intraparticle profiles; compact solutions are thus obtained both in the presence and absence of fast reactions. Calculations for a six-component catalytic reforming system show that the catalyst performance is strongly affected by intraparticle diffusion.

AMS (MOS) Subject Classifications: 34B15, 41A30, 65L10, 80A20, 80A30

Key Words: Multicomponent Diffusion, Catalysis, Chemical Reactions, Porous Media, Collocation, Stiff Equations, Approximation with Special Functions

Work Unit Number 2: Physical Mathematics

*Department of Chemical Engineering, University of Wisconsin-Madison, Madison, WI 53706

Sponsored by the United States Army under Contract No. DAAG29-80-C-0041.

SIGNIFICANCE AND EXPLANATION

Theoretical models of gas diffusion and flow in porous solids are well developed, and are beginning to be applied to simple catalytic systems. Calculations of this kind permit a new level of understanding of catalysis, which should lead to more efficient chemical processes.

Detailed simulations of catalyst particles should be especially useful in studies of multi-reaction processes, for which the catalyst selectivity may be sensitive to intraparticle diffusion. In this paper we summarize the relevant transport equations and give a new collocation method for solving this kind of problem.

The simulation of a catalyst particle needs to be done efficiently if it is to be included in a reactor computation. Collocation methods based on global polynomials become inefficient in the presence of fast reactions because of the steep reaction fronts which then occur. Improved basis functions are introduced here from a linearized version of the transport equations, thus providing compact solutions over a wide range of reaction rates.

COLLOCATION ANALYSIS OF MULTICOMPONENT DIFFUSION AND REACTIONS IN POROUS CATALYSTS

Jan P. Sørensen and Warren E. Stewart*

INTRODUCTION

Theoretical models of gas diffusion and flow in porous solids are well developed [23, 24, 10, 11, 17], and are beginning to be applied to simple catalytic systems [2, 9, 15, 18, 19, 20, 38]. Calculations of this kind permit a new level of understanding of catalysis, which should lead to more efficient chemical processes.

Detailed simulations of catalyst particles should be especially useful in studies of multi-reaction processes, for which the catalyst selectivity may be sensitive to intraparticle diffusion. In this paper we summarize the relevant transport equations and give a new collocation method for solving this kind of problem.

*Department of Chemical Engineering, University of Wisconsin-Madison, Madison, WI 53706

Sponsored by the United States Army under Contract No. DAAG-29-80-C-0041.

The simulation of a catalyst particle needs to be done efficiently if it is to be included in a reactor computation. Collocation methods based on global polynomials become inefficient in the presence of fast reactions [35, 26, 7, 36] because of the steep reaction fronts which then occur. Improved basis functions are introduced here from a linearized version of the transport equations, thus providing compact solutions over a wide range of reaction rates.

TRANSPORT EQUATIONS

Consider the steady diffusion and reaction of a multicomponent gaseous mixture in a porous catalyst particle. We use the following model [24, 10, 11] to describe the intraparticle molar fluxes:

$$\underset{\sim}{N}^{(m)} = - \sum_{k=1}^{n_w} (W_k/RT)\, [\underset{\sim}{F}(r_k)]^{-1} \underset{\sim}{\nabla} p - (B_0/\mu)\, c \underset{\sim}{\nabla} p - \underset{\sim}{D}_s \underset{\sim}{\nabla} c \qquad (1)$$

The first right-hand term arises from gaseous diffusion, the second from viscous flow, and the third from surface diffusion. The gaseous diffusion expression includes the leading thermal transpiration term $n_i \partial \ln T/\partial z$ from the dusty-gas model of Mason *et al.* [23]. The elements of $\underset{\sim}{F}(r_k)$ are obtained by setting $r = r_k$ in the expressions

$$F_{ii}(r) = 1/\mathcal{D}_{iK}(r) + \sum_{\substack{h=1 \\ h \neq i}}^{n_c} c_h/c\mathcal{D}_{ih} \qquad (2a)$$

$$i = 1, \ldots n_c$$

$$j = 1, \ldots n_c$$

$$F_{ij}(r) = - c_i/c\mathcal{D}_{ij} \qquad i \neq j \qquad (2b)$$

in which n_c is the number of gaseous species.

Equation (1) includes the Knudsen diffusion equation and the Stefan-Maxwell equation [6, 16] as asymptotes for low and high pressures, respectively. This model has also been tested thoroughly over the intermediate region [10, 11] commonly encountered in industrial gas-solid processes. The summation on k in eqn (1) is a quadrature of the flux expressions of Mason et al. [24] over the pore size distribution. A two-point sum ($n_w = 2$) fits the available data well for a variety of catalysts [10, 11]; one point suffices for narrow pore size distributions.

Equation (1) was developed for non-reacting systems, under the assumption that the concentrations and temperatures in the pores conform to smooth fields defined throughout the porous medium. For simplicity we use the same model in the presence of chemical reactions. This approach should be satisfactory if the pores are cross-linked frequently, so that the concentration changes along individual pore segments are small. This point is discussed in greater detail by Jackson [17]; see also Mingle and Smith [25].

The energy flux within the particle is modelled as

$$\underset{\sim}{N}_E = \sum_{i=1}^{n_c} \underset{\sim}{N}_i \bar{H}_i - k_{eff} \nabla T \qquad (3)$$

that is, as a sum of convective and conductive terms, with the Dufour effect [6] neglected.

In the following calculations, we use the interstitial concentrations c_i and the temperature T as state variables. Equations (1) and (3) are readily rewritten in these variables by insertion of the ideal gas law. The result can be expressed in the matrix form

$$\underset{\sim}{N} = - \underset{\sim}{D} \underset{\sim\sim}{\nabla} \underset{\sim}{\xi} \tag{4}$$

The flux array $\underset{\sim}{N}$ has the elements $\{\underset{\sim}{N}_1, \ldots \underset{\sim}{N}_{n_c}, \underset{\sim}{N}_E\}$, and the state vector $\underset{\sim}{\xi}$ has elements $\{c_1, \ldots c_{n_c}, T\}$. The elements of $\underset{\sim}{D}$ are summarized in Appendix A.

At steady state, the fluxes in the particle satisfy the mass and energy balances

$$\left(\underset{\sim\sim}{\nabla} \cdot \underset{\sim}{N}_i\right) = R_i \qquad i = 1, \ldots n_c \tag{5}$$

$$\left(\underset{\sim\sim}{\nabla} \cdot \underset{\sim}{N}_E\right) = R_E = 0 \tag{6}$$

in the smooth-field approximation. Here R_i is the local production rate of species i per unit volume of the heterogeneous medium; its evaluation for fairly general kinetics is discussed in [33].

In this work, we consider symmetric states $\{c_i(z^2), T(z^2)\}$ in a catalyst slab or sphere, with boundary conditions

$$c_i \Big|_{z=1} = c_{iO}; \qquad dc_i/dz \Big|_{z=0} = 0 \qquad i = 1, \ldots n_c \tag{7}$$

$$T \Big|_{z=1} = T_O; \qquad dT/dz \Big|_{z=0} = 0 \tag{8}$$

The dimensionless coordinate z is measured from the particle center, as a fraction of the particle half-thickness L. More general boundary conditions are readily accomodated.

A collocation procedure for solving eqns (4)-(8) is described in the next four sections. After the description, three numerical examples are given.

BASIS FUNCTIONS

The collocation procedure requires a set of basis functions to describe the concentration and temperature profiles. Global polynomials are often used for this purpose [35, 12, 36], but many terms are then required to get acceptable accuracy for fast reactions. Piecewise polynomials (splines) are more flexible [26, 7, 36], but the choice of breakpoints for these functions needs further study, especially for multicomponent problems. The approach taken here is to develop natural basis functions from a linearized form of the given problem. A similar approach has been applied successfully to systems of first-order differential equations [13].

Insertion of eqn (4) into (5) and (6), and linearization around a reference state $\underset{\sim}{\xi}_R$, gives the matrix differential equation

$$-\underset{\sim}{D}(\underset{\sim}{\xi}_R)\,\underset{\sim}{\nabla}^2\underset{\sim}{\xi} = \underset{\sim}{R}(\underset{\sim}{\xi}_R) + \underset{\sim}{R}'(\underset{\sim}{\xi}_R)\,[\,\underset{\sim}{\xi} - \underset{\sim}{\xi}_R\,] \qquad (9)$$

Here $\underset{\sim}{D}(\underset{\sim}{\xi}_R)$ is the transport coefficient matrix calculated at $\underset{\sim}{\xi}_R$ from the relations in Appendix A, $\underset{\sim}{R}(\underset{\sim}{\xi}_R)$ is the vector of production rates at $\underset{\sim}{\xi}_R$, and $\underset{\sim}{R}'(\underset{\sim}{\xi}_R)$ is the matrix $\partial\underset{\sim}{R}/\partial\underset{\sim}{\xi}$ evaluated at $\underset{\sim}{\xi}_R$ from the given kinetic model. The matrix $\underset{\sim}{D}(\underset{\sim}{\xi}_R)$ is non-singular, since eqns (1) and (3) are linearly independent [31].

The solution vector $\underset{\sim}{\xi}$ of eqns (7)-(9) is a linear combination of the following functions:

$$\begin{aligned} &1,\quad \cosh(z\sqrt{\lambda_k}) && \text{(Slab)} && k = 1, \ldots r \\ &1,\quad \sinh(z\sqrt{\lambda_k})/z && \text{(Sphere)} && k = 1, \ldots r \end{aligned} \qquad (10)$$

Here r is the rank of the matrix $[-\underset{\sim}{D}(\underset{\sim}{\xi}_R)^{-1}\,L^2\,\underset{\sim}{R}'(\underset{\sim}{\xi}_R)\,]$, and $\lambda_1, \cdots \lambda_r$ are its nonzero eigenvalues. If a p-fold eigenvalue yields

fewer than p eigenvectors, alternative functions given in eqn (11a) or (11b) will appear. Since in practice the rank may be uncertain, we use its upper bound m: the maximum number of independent production rates R_i permitted by the stoichiometry and local constraints of the reaction system [3, 16, 17, 31, 33]. In the stoichiometric analysis of [33], m is the number of non-equilibrium reactions that yield pivot coefficients for mobile species. The m largest values of Real($\sqrt{\lambda_k}$) are then used to obtain m functions of the form in eqn (10).

The quantities $\sqrt{\lambda_k}$ are generalized Thiele moduli [4] for the corresponding eigenfunctions in eqn (10). Polynomial approximations of the linearized solution become difficult if any of these moduli are large; in such cases we will say that the differential equations are "stiff".

Equation (10) is written for non-zero eigenvalues $\lambda_1, \cdots \lambda_m$, i.e., for kinetics of full rank m. In this case, the spatial function "1" corresponds to an equilibrium solution $\underset{\sim}{\xi}_e$ of eqn (9). If any of $\lambda_1, \cdots \lambda_m$ in eqn (10) are zero, then the corresponding functions are replaced by z^{2k}, obtained by expansion of the solutions in powers of $\sqrt{\lambda}$. This procedure provides a particular solution proportional to z^2 whenever eqn (9) lacks an equilibrium solution; in such cases, the function "1" is merely a solution of the related homogeneous equation, $\underset{\sim}{\nabla}^2\underset{\sim}{\xi} = \underset{\sim}{0}$. Kinetics of rank less than m can arise from zero-order rate expressions (which we prefer to avoid), or from other causes such as absence of various concentrations from the reaction rate expressions.

For non-linear problems, we extend the function set of eqn (10) by differentiation with respect to $\sqrt{\lambda}$ at each characteristic value λ_k. The following differential forms are convenient:

$$\left(1 - \frac{\partial}{\partial\sqrt{\lambda}}\right)^s \cosh(z\sqrt{\lambda}) \Bigg|_{\lambda_k} = \frac{(1-z)^s}{2} \exp(z\sqrt{\lambda_k}) + \frac{(1+z)^s}{2} \exp(-z\sqrt{\lambda_k})$$

$$s = 1, 2, \ldots \qquad \text{(Slab)} \qquad (11a)$$

$$\left(1 - \frac{\partial}{\partial\sqrt{\lambda}}\right)^s \frac{\sinh(z\sqrt{\lambda})}{z} \Bigg|_{\lambda_k} = \frac{(1-z)^s}{2z} \exp(z\sqrt{\lambda_k}) - \frac{(1+z)^s}{2z} \exp(-z\sqrt{\lambda_k})$$

$$s = 1, 2, \ldots \qquad \text{(Sphere)} \qquad (11b)$$

These functions are also used to deal with clustered eigenvalues as described below. The solutions $\xi_i(z)$ and $N_{iz}(z)$ are then approximated as combinations of basis functions selected from eqns (10) and (11),

$$\tilde{\xi}_i = \sum_{j=0}^{n} a_{ij}\, \phi_j(z) \qquad i = 1, \ldots n_c+1 \qquad (12)$$

$$\tilde{N}_{iz} = \sum_{j=1}^{n} f_{ij} \frac{d}{dz} \phi_j(z) \qquad i = 1, \ldots n_c+1 \qquad (13)$$

with adjustable coefficients a_{ij} and f_{ij}, and with $\phi_0(z) = 1$. The index n is chosen by the user. Here and below, we mark the approximate solutions with a tilde (~). Equation (13) is included to facilitate the treatment of eqns (5) and (6) for systems with variable $\underset{\sim}{D}$.

For sufficiently large n, eqn (12) can approximate any continuous symmetric function $\xi_i(z^2)$ to arbitrary accuracy over the interval [0,1], even if all the values $\sqrt{\lambda_k}$ are replaced by a single constant α. To prove this, we note that eqn (12) then reduces to a representation of $(\xi_i - a_{i0})$ [Slab] or $z(\xi_i - a_{i0})$ [Sphere] by an expansion $P_n(1-z)\exp(\alpha z) + P_n(1+z)\exp(-\alpha z)$. Division by $\exp(\alpha z)$ leads, for either geometry, to a representation of a continuous function by a polynomial $P_n(1-z)$; the proof then follows directly from the

Weierstrass approximation theorem [8]. Equation (13) has similar approximating power for the fluxes N_{iz}. Consequently, it is permissible to modify the λ's for simplicity if a sufficient number of basis functions is used.

The following ordering of the functions for selection has given good results. Let the desired number of collocation points be n; then n+1 functions $\phi_i(z)$ are required. We start with $\phi_0(z) = 1$ and $\alpha_0 = 0$; then we choose the constants $\alpha_1, \ldots \alpha_m$ as the values of $\text{Real}(\sqrt{\lambda_k})$ in descending order. These values are necessarily non-negative. If $n < m$, we drop the values after α_n, thus omitting those terms of the linearized solution. On the other hand, if $n > m$, we insert $\alpha_{m+1}, \ldots \alpha_n$ according to the recursion formula $\alpha_j = \alpha_{j-m}$. Then we rearrange and relabel the resulting list to form an ascending sequence $\{\alpha_j\} = \{\alpha_0, \ldots \alpha_n\}$.

Close groups of unequal α values are then compacted as follows, to strengthen the linear independence of the basis functions. If any $\alpha_j \leq 2.0j$ for a slab, or $\alpha_j \leq 2.5j$ for a sphere, with $\alpha_{j-1} < \alpha_j$, then α_j and all equal or smaller α's are replaced by zeros, thus replacing those basis functions by polynomials. Subsequent sequences $\{\alpha_h, \ldots \alpha_{h+k}\}$, with k the largest integer such that $\alpha_{h+k}/\alpha_h \leq (1.4)^{k-1}$, are compacted by replacing each member with $(\alpha_h\, \alpha_{h+1} \cdots \alpha_{h+k})^{1/k}$. These procedures were developed from numerical tests to provide a well-conditioned Gram-Schmidt solution of eqn (19).

The basis functions are then obtained by rewriting eqns (10) and (11) as follows, with multipliers $\exp(-\alpha_j)$ to ensure computable values:

For $\alpha_j = 0$ in a slab or sphere,

$$\phi_j = z^{2s_j} \tag{14a}$$

For $\alpha_j > 0$ in a slab,

$$\phi_j = \frac{(1-z)^{s_j}}{2} \exp[\alpha_j(z-1)] + \frac{(1+z)^{s_j}}{2} \exp[-\alpha_j(z+1)] \tag{14b}$$

For $\alpha_j > 0$ in a sphere,

$$\phi_j = \frac{(1-z)^{s_j}}{2z} \exp[\alpha_j(z-1)] - \frac{(1+z)^{s_j}}{2z} \exp[-\alpha_j(z+1)] \tag{14c}$$

Each integer s_j is taken here here as the number of prior occurrences of the associated value α_j in the α-list.

The selection order used here is different from that used by Guertin et al., who gave last priority to rapidly decaying functions in their basis selection for initial value problems. Such a rule is not relevant for the boundary-value problems considered here, in which the fluxes depend on the gradients and thus the steep basis functions may be important. By giving priority to the large α's (after α_0), we bracket any unused values and obtain good accuracy with fewer basis functions.

COLLOCATION POINTS

The collocation procedure consists of adjusting eqns (12) and (13) to satisfy eqns (7) and (8) exactly, and to satisfy eqns (4)-(6) at a set of interior points $z_1, \ldots z_n$. We choose these points by analyzing the residuals of eqns (5) and (6),

$$\mathcal{F}_i \underset{\sim}{\xi} = \frac{1}{z^a} \frac{d}{dz} [\, z^a \underset{\sim}{N}_{iz}(\underset{\sim}{\xi})] - L\, R_i(\underset{\sim}{\xi}) \qquad i = 1, \ldots n_c+1 \tag{15}$$

in the series form

$$\mathcal{F}_i \tilde{\xi} = Q_n(z) \sum_{k=0}^{\infty} d_{ik} \phi_k(z) \qquad i = 1, \ldots n_c+1 \qquad (16)$$

Here the d_{ik} are unknown coefficients, and $Q_n(z)$ is a function whose zeros $z_1, \ldots z_n$ will be the interior collocation points. We choose

$$Q_n(z) = \phi_n(z) + \sum_{j=0}^{n-1} b_j \phi_j(z) \qquad (17)$$

in which the b_j are coefficients to be determined.

We minimize the magnitudes of the mean residuals

$$\int_0^1 \mathcal{F}_i \tilde{\xi} \, z^a \, dz = N_{iz}(1) - L \int_0^1 R_i(\tilde{\xi}) \, z^a \, dz$$

$$= \int_0^1 \sum_{k=0}^{\infty} d_{ik} Q_n(z) \phi_k(z) \, z^a \, dz \qquad i = 1, \ldots n_c+1 \qquad (18)$$

with respect to the coefficients b_j by imposing the following orthogonality conditions on $Q_n(z)$:

$$\int_0^1 Q_n(z) \phi_k(z) \, z^a \, dz = 0 \qquad k = 0, \ldots n-1 \qquad (19)$$

These conditions cause $Q_n(z)$ to have n distinct zeros on the interval (0,1), as shown in Appendix B. Collocation at the zeros of $Q_n(z)$ thus is feasible, and eliminates the first n terms of the mean residuals as expressed in eqn (18). The coefficients b_j in eqn (17) are determined by eqn (19); the values of the d_{ik} are not required.

Equations (19) are also obtainable by minimizing the mean square of $Q_n(z)$ with respect to $b_0, \ldots b_{n-1}$. The leading term of each

residual $\mathcal{F}_i \tilde{\xi}$ in eqn (16) is thus minimized in a least-squares sense over the interior of the catalyst particle.

In systems with constant $\underset{\sim}{D}$, eqns (13) are exactly consistent with eqns (12) and (4). In systems with variable $\underset{\sim}{D}$, however, flux residuals $\tilde{N}_{iz} - \underset{\sim}{D}_i(\tilde{\xi})\, d\tilde{\xi}/dz$ arise. The resulting truncation error in eqn (20) is normally small, and could be reduced by using a second set of points for evaluation of $\tilde{N}_{iz}$. This question will be considered at another time.

DISCRETE-ORDINATE EQUATIONS

It is convenient to compute the solution values directly at the collocation points, rather than solve for the coefficients in eqns (12) and (13). This is done by expressing the gradient and divergence operations in the forms

$$\left.\frac{d\tilde{\xi}_i}{dz}\right|_{z_k} = \sum_{j=1}^{n+1} A_{kj}\, \tilde{\xi}_i(z_j) \qquad (20)$$

$$\left.\frac{1}{z^a}\frac{d}{dz}\left(z^a \tilde{N}_{iz}\right)\right|_{z_k} = \sum_{j=1}^{n} E_{kj}\, \tilde{N}_{iz}(z_j) \qquad (21)$$

with a = 0 for slabs and a = 2 for spheres. Equation (21) has n terms, as does eqn (13); for simplicity the needed n values of $\tilde{N}_{iz}$ are taken at the interior points $z_1, \ldots z_n$. A similar divergence operator was used by Feng [9] for effectiveness-factor calculations with polynomial basis functions.

Application of eqns (20) and (21) to eqns (12) and (13) gives the linear equations

$$\left[\left.\frac{d\phi_i}{dz}\right|_{z_k}\right] = \left[A_{kj}\right]\left[\phi_i(z_j)\right] \qquad \begin{matrix} i = 0, \ldots n \\ j = 1, \ldots n+1 \\ k = 1, \ldots n+1 \end{matrix} \tag{22}$$

$$\left[\left.\frac{1}{z^a}\frac{d}{dz}\left(z^a \frac{d\phi_i}{dz}\right)\right|_{z_k}\right] = \left[E_{kj}\right]\left[\left.\frac{d\phi_i}{dz}\right|_{z_j}\right] \qquad \begin{matrix} i = 1, \ldots n \\ j = 1, \ldots n \\ k = 1, \ldots n \end{matrix} \tag{23}$$

from which the matrices $[A_{kj}]$ and $[E_{kj}]$ for the given problem are calculated.

Insertion of eqns (20) and (21) into eqns (4)-(6) then gives the collocation equations

$$-L\,\tilde{N}_{iz}(z_k) = \sum_{j=1}^{n_c} D_{ij}\left(\tilde{\xi}(z_k)\right) \sum_{h=1}^{n+1} A_{kh}\,\tilde{\xi}_j(z_h) \tag{24}$$

$$\sum_{j=1}^{n} E_{kj}\,L\,\tilde{N}_{iz}(z_j) = L^2\,R_i\left(\tilde{\xi}(z_k)\right) \tag{25}$$

$$i = 1, \ldots n_c+1 \qquad k = 1, \ldots n$$

Insertion of eqn (24) into the left side of (25) gives a system of equations for the mesh-point values $\tilde{\xi}_i(z_k)$; we solve this system by Newton's method. The symmetry of the problems considered here would allow replacing some of eqns (25) by stoichiometric relations among the fluxes [31]; however, the equations as shown allow a simpler extension to non-symmetric problems.

If equilibrium reactions or immobile species are included in the reaction scheme, then a corresponding number of differential equations must be replaced by local equations as in [33]. These changes do not arise in the examples considered here.

COMPUTATION PROCEDURE

A reference state $\underset{\sim}{\xi}_R$ was chosen for each problem as described in Examples 1-3 below. The maximum number of independent production rates, m, was computed as described under eqn (10). The matrices $\underset{\sim}{D}(\underset{\sim}{\xi}_R)$ and $\underset{\sim}{R}'(\underset{\sim}{\xi}_R)$ were computed analytically from the expressions for the fluxes and reaction rates, and the eigenvalues of $[-\underset{\sim}{D}^{-1}(\underset{\sim}{\xi}_R)\, L^2\, \underset{\sim}{R}'(\underset{\sim}{\xi}_R)]$ were computed by the Q-R method. Single precision (8 digits) sufficed up to this point.

The function $Q_n(z)$ was determined from eqns (17) and (19) by a modified Gram-Schmidt algorithm. The zeroes of $Q_n(z)$ were found by a grid search and Newton iteration. The weight matrices $[A_{kj}]$ and $[E_{kj}]$ were then computed from eqns (22) and (23) by LU decomposition [30] with partial pivoting. These calculations were done in double precision (18 digits). Polynomial collocation was initiated in the same way except that the eigenvalues were replaced by zeros.

Equations (24) and (25) were then set up in single precision and solved by Newton's method, starting from estimates $\xi_i(z_k)$ based on a one-point solution. The examples that follow were solved with a general-purpose program, which does the calculations automatically when the desired reaction model and conditions are presented in digital form.

EXAMPLE 1. SECOND ORDER REACTION WITH LARGE THIELE MODULUS

As our first example we consider an isothermal, irreversible second-order reaction in a porous catalytic slab. Solutions are obtained by collocation with the hyperbolic basis functions, and various alternative methods are compared.

The problem can be stated in dimensionless form as follows,

$$\frac{d^2c^*}{dz^2} = \phi^2 c^{*2} \qquad -1 < z < 1 \qquad (26)$$

$$c^* = 1 \quad \text{at} \quad z = \pm 1 \qquad (27)$$

and has one independent rate of production; thus, m = 1. The problem is non-linear and is stiff when the Thiele modulus, Φ, is large; it provides a good test of approximate solution methods. Solutions are given here for the dimensionless boundary flux, $N^* = dc^*/dz\big|_{z=1} = \Phi^2\eta$, at Thiele moduli of 10, 100, and 1000.

For these large values of Φ, the concentration will drop almost to zero at the center of the slab. Linearizing the reaction term of eqn (26) at the mean concentration of 0.5, we obtain the single eigenvalue $\lambda_1 = -\partial(\Phi^2 c^{*2})/\partial c^*\big|_{0.5} = \Phi^2$. The resulting basis functions, for $j \geq 1$, are

$$\phi_j = \frac{(1-z)^{j-1}\exp[(z-1)\Phi]}{2} + \frac{(1+z)^{j-1}\exp[-(z+1)\Phi]}{2} \qquad (28)$$

Several of these functions are shown in Figure 1.

Table 1 shows the convergence of the approximations to the boundary flux N^* with increasing number of collocation points. The hyperbolic functions of eqn (28) give rapid convergence throughout. With these functions, two-point collocation gives the boundary flux within about 1 percent for Thiele moduli $\Phi \geq 10$.

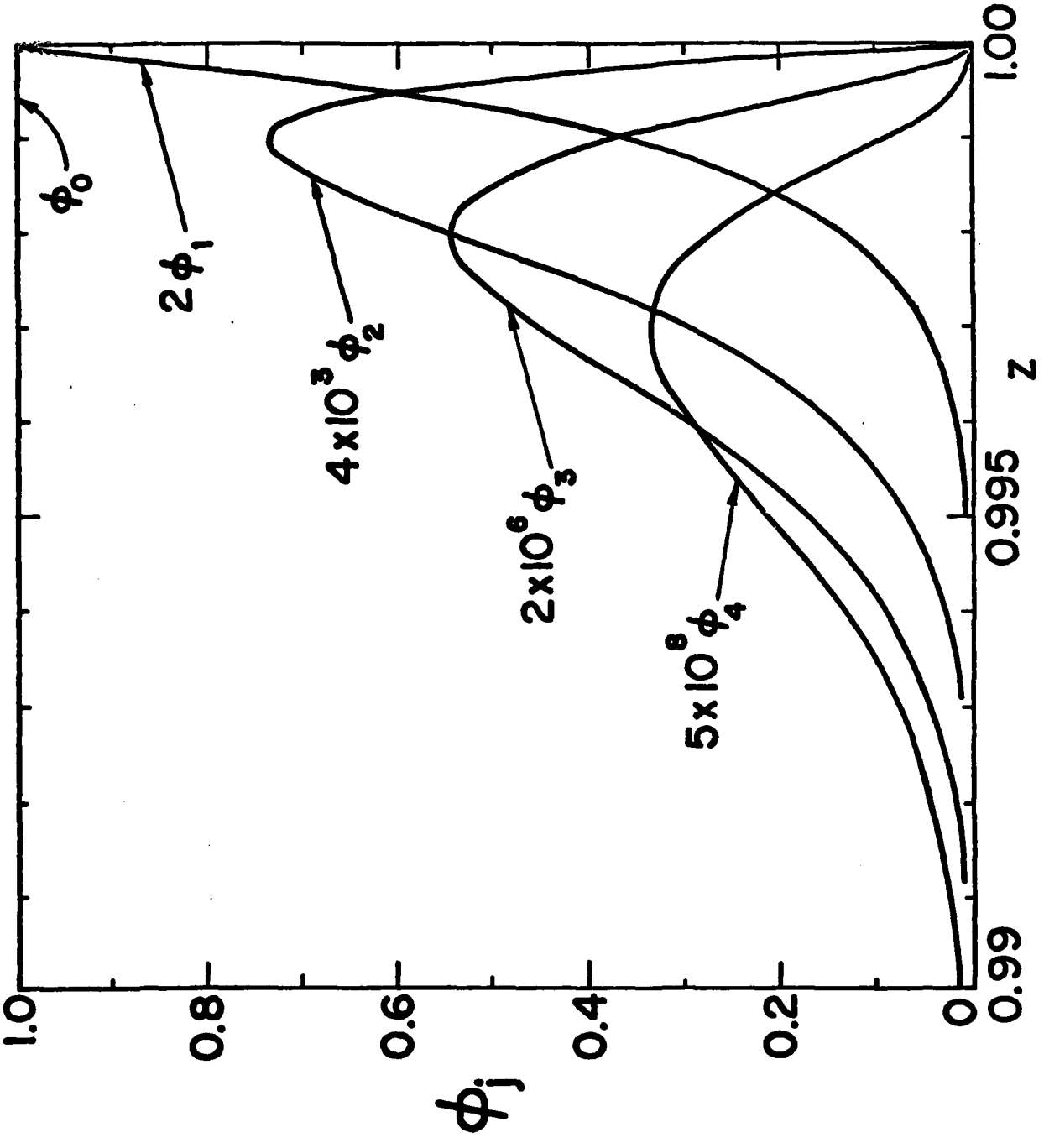

Figure 1. Basic functions $\phi_j(z)$ of eqns (14a) and (28) for Example 1 with Thiele modulus of 1000.

TABLE 1

Convergence of Solutions for Boundary Flux, $N^* = \phi^2\eta$,

for Isothermal Second-Order Reaction in a Slab

Number of Collocation Points	Results with hyperbolic functions			Results with splines [36]
	$\Phi = 10$	$\Phi = 100$	$\Phi = 1000$	$\Phi = 1000$
1	7.9736	91.356	969.83	627.5
2	8.0537	81.127	814.16	708.5
3	8.1505	81.639	817.65	715.8
4	8.1614	81.662	816.79	792.5
5	8.1637	81.661	816.67	800.4
6	8.1641	81.654	816.57	812.0
7	8.1642	81.652	816.53	815.2
8	8.1642	81.651	816.51	815.5
9	8.1642	81.650	816.51	——
10	8.1642	81.650	816.50	——
11	8.1642	81.650	816.50	——
—	(8.16421)#	(81.6496)#	(816.497)#	(816.497)#

#From the general solution for a single reaction in a slab [5, 27, 3].

The exact concentration profile at $\Phi = 1000$ is shown in Figure 2 along with point values computed by the present method. Good agreement is found at each $n > 1$ except for the point of lowest concentration, where the linearization of the second-order kinetics is least realistic. Note that each set of collocation points is positioned nicely in the reaction zone.

Villadsen and Michelsen [36] have analyzed this problem by collocation with global and piecewise polynomials. Using global polynomials at $\Phi = 100$, they obtained a boundary flux of 100.0 for $n = 8$, and 83.9 for $n = 12$. From Table 1 we see that the hyperbolic functions give more accurate values than these, even for n as small as 2.

Piecewise polynomials (splines) were used by Villadsen and Michelsen [36] to solve this problem at $\Phi = 1000$, where global polynomials failed. The general solution for single reaction in a slab [5, 27, 3] was used to select the breakpoints of the piecewise polynomials. Their best results are shown in Table 1; these were obtained with a breakpoint at $z = 0.9987$ for $n \geq 1$, and another at $z = 0.991$ for $n \geq 4$. Comparing the last two columns of Table 1, we see that each hyperbolic solution (except for $n = 1$) approximates N^* more accurately than the 2n-point solution based on splines.

The problem for $\Phi = 1000$ may also be solved by a modified Paterson-Cresswell method. In the original method [26], the reaction is assumed to be so fast that the concentration in an interior region $[0,z_s]$ may be neglected, and eqn (5) need only be integrated over the region $[z_s,1]$. In the modified method [36] the concentration gradient, rather than the concentration itself, is neglected in the region $[0,z_s]$, and the boundary condition at $z = z_s$ becomes $dc/dz = 0$

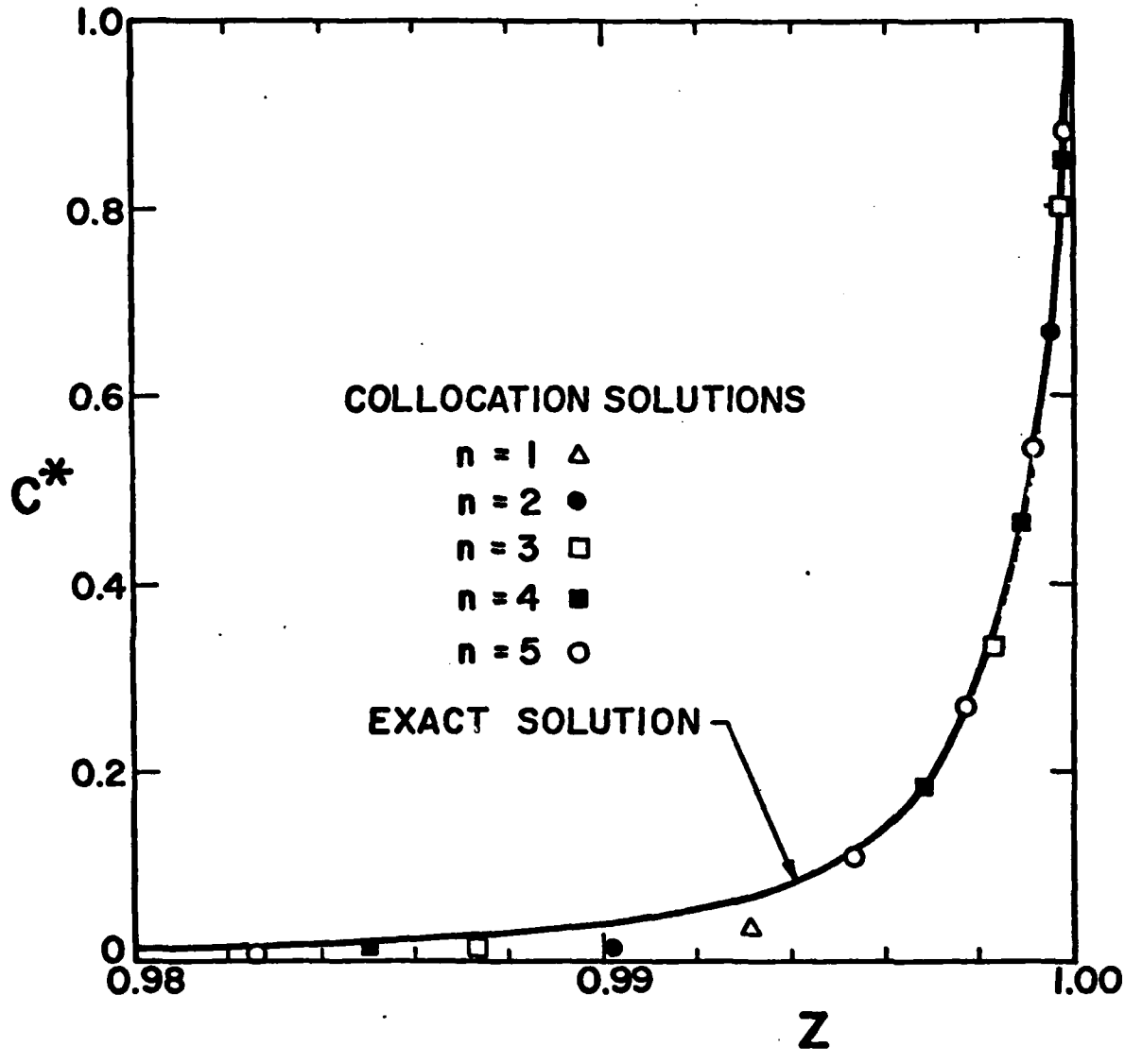

Figure 2. Concentrations in a catalyst slab with isothermal second-order reaction at Thiele modulus of 1000. The collocation solutions are based on the functions of eqn (28), along with $\phi_0(z) = 1$.

rather than c = 0. With polynomial collocation, some experimentation is needed to select a suitable value of z_s; however, with the hyperbolic functions, the choice of z_s is not so critical.

For a chosen z_s we compute a solution with a modified Thiele modulus $\phi_s = (1 - z_s)\phi$. Let the modified boundary flux be N_s^*; then the boundary flux of the original problem becomes $N^* = N_s^*/(1 - z_s)$. To obtain the boundary flux for $\phi = 1000$, we first try $z_s = 0.9$ which gives $\phi_s = 100$. Then $N_s^* = 81.7$ (Table 1, $n \geq 3$), and $N^* = 817.$; this is comparable to the result obtained from our global procedure. The alternate choice $z_s = 0.99$ gives $\phi_s = 10$, whence $N_s^* = 8.16$ (Table 1, $n \geq 4$), and $N^* = 816$. Both choices of z_s give good approximations of the exact flux $N^* = 816.497$; however, the direct solution shown in Table 1 is at least as quick.

EXAMPLE 2. THE WEISZ-HICKS PROBLEM

As a second test of the new collocation procedure, we consider the non-isothermal effectiveness-factor problem of Weisz and Hicks [37]. This problem is described by eqns (4)-(8) with spherical symmetry, constant transport properties, and a first-order Arrhenius kinetic model.

The kinetic model chosen for this example is $R_2 = -R_1 = c_1^* \exp[-15000*(1/T - 1/500)]$. Here again, m = 1. The other chosen values are $W_k = 0$, $B_0 = 0$, $D_{ijs} = \delta_{ij}$, L = 3, $k_{eff} = 1$, $\Delta H = -100$, $c_0 = 1$, and $T_0 = 500$ in eqns (1) and (3)-(8). These values make $\underset{\sim}{D}$ a unit matrix, and correspond to $\phi = 3$, $\beta = 0.2$, and $\gamma = 30$ in the notation of Weisz and Hicks [37].

For this single-reaction problem, eqns (4)-(8) yield the steady state relation $(T - T_0)/T_0 = (1 - c^*)\beta$ throughout the particle. Equation (5) then reduces to the form [37]

$$\frac{1}{z^2}\frac{d}{dz}\left(z^2 \frac{dc^*}{dz} \right) = \phi^2 R^*(c^*) \qquad (29)$$

with

$$R^*(c^*) = c^* \exp\left[\frac{\gamma\beta(1 - c^*)}{1 + \beta(1 - c^*)}\right] \qquad (30)$$

This function is plotted in Figure 3 for the chosen values of β and γ.

The multiplicity criteria of Luss [22], as well as those of Stewart and Villadsen [32], predict a strongly ignited steady state. Thus, the reactant concentration will span the range of Figure 3, and the reaction rate will have a strong peak within the particle.

A linearized solution (n = m) will clearly not be adequate here; the added basis functions of eqn (11) will be essential. The region to the left of the peak in Figure 3 is chosen for the linearization, in order to describe accurately the inner border of the reaction zone. Linearization at $c^* = 0$ gives $\lambda_1 = 1336.$, whereas an orthogonal linear fit of the rate function in the region of positive slope gives $\lambda_1 = 457.8$. Linearization at a point to the right of the peak (as would be appropriate for an unignited particle) gives a negative, real λ_1 and yields polynomial basis functions according to the selection rules described above.

Table 2 shows the convergence of the solutions for the boundary flux. Both hyperbolic function sets give good results for n > 3; the set based on $c_R^* = 0$ is preferred. To obtain better than 2 percent accuracy with this set we need only 4 collocation points, whereas with polynomials 9 points are required.

EXAMPLE 3. CATALYTIC REFORMING OF C7 HYDROCARBONS

Krane and co-workers [21] gave a kinetic model for catalytic

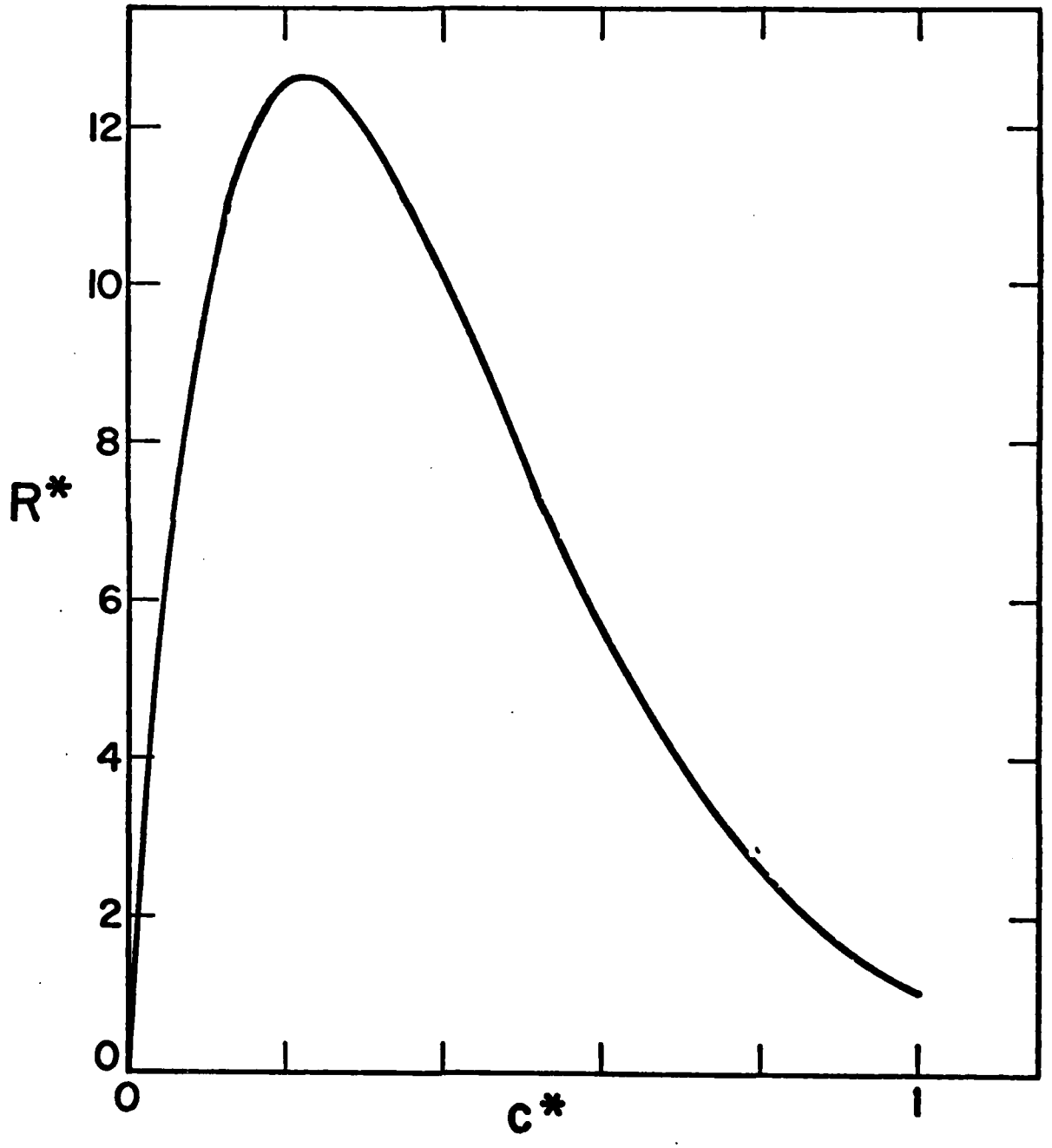

Figure 3. Steady-state rate function of eqn (30) for the Weisz-Hicks problem with $\beta = 0.2$ and $\gamma = 30$.

TABLE 2

Convergence of Solutions for Boundary Flux for the Weisz-Hicks Problem with $\Phi = 3.$, $\beta = 0.2$ and $\gamma = 30.$

Number of Collocation Points, n	Collocation Solutions, $\tilde{N}^* = \Phi^2 \tilde{n}/3$		
	Hyperbolic functions		Polynomials
	$\alpha_i = \sqrt{1336.}$ #	$\alpha_i = \sqrt{457.8}$ ##	$\alpha_i = 0$
	i > 0	i > 0	all i
1	33.524	22.012	4.942
2	12.148	7.828	12.935
3	8.583	10.418	6.661
4	9.655	8.830	7.317
5	9.337	9.573	9.218
6	9.500	9.546	10.359
7	9.438	9.371	9.130
8	9.447	9.428	9.209
9	9.456	9.475	9.546
10	9.451	9.459	9.502
11	9.450	9.443	9.406
12	9.451	9.448	9.445
13	9.451	9.453	9.465

Determined by linearization at $c^* = 0$.

Determined from a least-squares linear fit of $R^*(c^*)$ over the region of positive slope in Figure 2.

reforming of C7 hydrocarbons over platinum-alumina. Their reaction scheme is as follows:

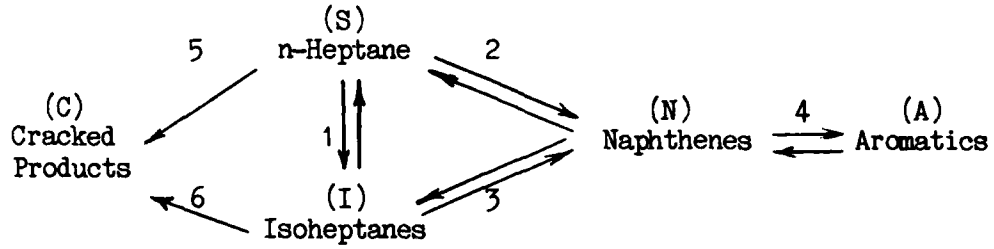

Their pseudo-homogeneous rate expressions have been generalized by Guertin et al. [13], with the equilibrium constants K_1, K_2, and K_3 recalculated from the API tables [1] for self-consistency. For those calculations and the following ones, species A was taken as toluene, C as an equimolar mixture of propane and i-butane, N as methylcyclohexane, and I as an equimolar mixture of 2- and 3-methylhexane.

The present theory requires local kinetic expressions, rather than pseudo-homogeneous ones. To obtain these, we have adjusted the rate constants to obtain mean rates $\langle R_i \rangle$ consistent with those of Krane et al. at the conditions of their experiments. A particle diameter of 1/16" and length of 3/32" were assigned to those experiments after consultation with John Sinfelt; this gives an effective sphere radius of 0.9 mm by the Wheeler-Aris rule [3, p. 162]. Activation energies of 15,000 K were assumed for the forward reactions; these values are not critical since the temperature corrections required are small.

The transport parameters for a similar catalyst have been determined by Feng [9] by fitting eqn (1) to his mass flux experiments. A one-point lumping of the pore size distribution gave $W_1 = 0.081479$ and $r_1 = 374$ A, whereas a two-point lumping gave $W_1 = 0.11803$, $r_1 = 64$ A, $W_2 = 0.032828$, and $r_2 = 845$ A; in both cases a

permeability $B_0 = 4.5\ 10^{-6}$ g cm sec^{-2} atm^{-1} was obtained. A thermal conductivity $k_{eff} = 0.0005$ cal cm^{-1} sec^{-1} K^{-1} is given by Sehr [29] for a similar catalyst; this value was used for the non-isothermal cases. A catalyst density of 1.22 g cm^{-3} was used, as for Feng's experiments.

The transport coefficients μ and $\mathcal{D}_{ij}$ were calculated at 769.24 K from eqns (1.4-18,19) and (16.4-12,15,16) of Bird et al. [6]; for other temperatures a correction $(T/769.24)^{0.8}$ was applied. Lennard-Jones parameters were obtained for hydrogen from [6], and for each hydrocarbon from correlation (iii) of Tee et al. [34] with critical properties and vapor pressures from the API tables [1]. Surface diffusion was neglected.

From these physical data and the production rates $\langle R_i \rangle$ reported by Krane et al., we have obtained the following local rate equations for a temperature of 769.24 K (925 F):

$$\hat{R}_1 = 0.702\ p^{-0.63} [\ p_S - p_I/2.95\ ]$$

$$\hat{R}_2 = 0.567\ p^{-1} [\ p_S - p_H\ p_N/1.77\ ]$$

$$\hat{R}_3 = 0.567\ p^{-1} [\ p_I - p_H\ p_N(2.95/1.77)\ ]$$

$$\hat{R}_4 = 78.8\ p^{-1} [\ p_N - p_H^3\ p_A/377700.\ ] \qquad (31)$$

$$\hat{R}_5 = 0.106\ p^{-0.67}\ p_S$$

$$\hat{R}_6 = 0.061\ p^{-0.67}\ p_I$$

With these local expressions, the computed mean production rates $\langle R_i \rangle$

closely approximate the values reported in [21] for the n-heptane and methylcyclohexane conversion experiments.

The pseudo-homogeneous rate constants of Krane et al. [21, 13] differ from our local values by the following factors: 0.52 for reaction 1; 0.63 for reactions 2 and 3; 0.13 for reaction 4; 1.47 for reactions 5 and 6. These comparisons show that the intraparticle gradients are important, even for this small particle size. Similar conclusions were reached by Hettinger et al. [14] from their experiments with several particle sizes.

Calculations are reported here for catalytic reforming in spherical particles with the following boundary conditions at $z = 1$: $p_S = p_N = p_A = 1$ atm, $p_H = 15$ atm, $p_I = p_C = 0$, $T = 769.24$ K. The large naphthene partial pressure corresponds to a first-reactor inlet condition; the fate of the naphthenes in that region is crucial to the selectivity of the process. Calculations are given for spherical particles with radii of 0.9 and 1.6 mm; the latter size corresponds approximately to a 1/8" x 1/8" pelleted catalyst.

The reference state was chosen here as $\underset{\sim}{\xi}(z_1)$ from a one-point polynomial collocation solution; other choices of $\underset{\sim}{\xi}_R$ would give comparable results for this mildly non-linear reaction model. Analysis of the stoichiometry by the method of [31] gives $m = 4$ as the maximum number of independent production rates.

Table 3 shows the values λ_k and α_k for the 0.9 mm particle with a one-point pore size distribution model. The complex eigenvalues arise from the temperature dependence of the reaction rates; the eigenvalues were all real in the isothermal case.

Table 4 shows the convergence of the boundary fluxes for two species with increasing n; the efficiency of the hyperbolic functions is evident, especially for hydrogen. The fluxes of both species are

TABLE 3

Selection of Basis Functions for Catalytic Reforming in a Nonisothermal Particle. $L = 0.9$ mm and $n_w = 1$

k	Eigenvalues λ_k	Real($\sqrt{\lambda_k}$) $= \alpha_{k,initial}$	Selection Order(#) after $\alpha_0 = 0$
(*)	$-0.2\ 10^{-7}$	(*)	
(*)	$0.3\ 10^{-7}$	(*)	
(*)	$-0.00119 + 0.00443\ i$	(*)	
1	$-0.00119 - 0.00443\ i$	0.0474	4, 8, ...
2	$17.381 + 0.56871\ i$	4.1696	3, 7, ...
3	$17.381 - 0.56871\ i$	4.1696	2, 6, ...
4	422.57	20.556	1, 5, ...

(*) Since this problem has $m = 4$, the 4 largest values Re($\sqrt{\alpha}$) are selected. The other eigenvalues are not used.

(#) These are not the indices j of eqn (14); the latter are obtained by labeling the chosen α values in ascending order as $\alpha_0, \ldots \alpha_n$. The grouping operations are then performed.

TABLE 4

Convergence Test of Boundary Fluxes for Catalytic Reforming in a Nonisothermal Particle. $L = 0.9$ mm and $n_w = 1$

Number of Collocation Points	$L\tilde{N}_{iz}$, mole cm^{-1} sec^{-1} * 10^6			
	Hyperbolic functions		Polynomial functions	
	Hydrogen flux	n-Heptane flux	Hydrogen flux	n-Heptane flux
1	1.4274	-.06692	.3709	-.05133
2	1.4279	-.03992	.8670	-.04834
3	1.4343	-.04035	1.2421	-.04102
4	1.4350	-.04122	1.3945	-.03984
5	1.4309	-.04299	1.4293	-.04105
6	1.4297	-.04322	1.4322	-.04797
7	1.4286	-.04337	1.4304	-.04294
8	1.4279	-.04347	1.4290	-.04329
9	1.4279	-.04351	1.4282	-.04344

accurate within 1% for $n \geq 6$ with the hyperbolic functions, versus $n \geq 8$ with polynomials. Since the number of operations required to solve eqn (26) varies essentially as n^3, the hyperbolic functions give practical accuracy in about half the computing time.

Table 5 shows the mean production rates computed with n = 7, for several conditions and several versions of the transport equations. The first two lines give results for a nonisothermal 0.9 mm particle with n_w = 1 and 2 in eqn (1). The appreciable difference between these two cases is caused by the wide distribution of pore sizes in the catalyst. The next two lines are obtained for an isothermal particle with n_w = 1 and 2. As expected, there are only moderate differences between the non-isothermal and isothermal solutions because the net heat of reaction is small. Line 5 represents a simplified model in which all off-diagonal elements in the $\tilde{F}(r)$ matrix are neglected, thus giving each molar flux in the form $N_{iz} = - D_{ieff} dc_i/dz$. The resulting approximations for $\langle R_i \rangle$ are good within 10 percent; larger deviations may be expected for systems in which the gaseous phase is not so diluted with a highly mobile component.

Line 6 gives rates calculated with a permeability twice the measured value. These results agree closely with line 2; thus, approximate values of B_0 and μ should normally suffice.

Lines 7 and 8 give the mean production rates for larger and smaller particles: 1.6 mm and 0 mm. The rates, and their ratios, vary strongly with particle size; the rate for n-heptane actually changes sign. Thus, a pseudo-homogeneous kinetic model is not appropriate, at least for these reaction conditions.

Tables 6 and 7 show the concentration and temperature profiles for both particle sizes, calculated from the full model with n_w = 2.

TABLE 5

Mean Production Rates for Catalytic Reforming in Spherical Particles, Computed with n = 7

Specifications	L, mm	$\langle \hat{R}_i \rangle$, mole g^{-1} sec^{-1} * 10^6					
		n-Heptane	Iso-heptanes	Naphthenes	Hydrogen	Toluene	Cracked Products
Nonisothermal, n_w=1	0.9	-13.17	44.59	-191.5	433.7	156.9	6.91
Nonisothermal, n_w=2	0.9	-13.44	47.04	-202.7	458.2	165.8	6.98
Isothermal, n_w=1	0.9	-13.96	44.71	-193.5	440.6	159.2	7.16
Isothermal, n_w=2	0.9	-14.36	47.23	-205.0	466.2	168.6	7.26
Nonisothermal, D_{ieff} model(*), n_w=2	0.9	-13.81	48.80	-213.1	480.9	173.1	7.20
Nonisothermal, B_0 doubled, n_w=2	0.9	-13.40	47.03	-202.6	458.6	165.8	6.98
Nonisothermal, n_w=2	1.6	-9.43	27.53	-115.5	264.6	95.0	5.80
Small-particle limit	0.0	29.59	250.3	-1489.	3327.	1205.	8.49

(*) The D_{ieff} model is obtained by neglecting the right-hand term of eqn (2b).

TABLE 6

Profiles for Catalytic Reforming in a Spherical Particle of Radius 0.9 mm

Computed with $n = 7$ and $n_w = 2$

	Concentrations, mole $cm^{-3} * 10^6$						
z	n-Heptane	Iso-heptanes	Naphthenes	Hydrogen	Toluene	Cracked Products	Temp. K
1.0000	15.84	0.	15.84	237.6	15.84	0.	769.24
0.9904	15.50	0.69	13.00	238.2	17.88	0.07	768.80
0.9488	14.13	2.79	5.70	239.6	23.17	0.38	767.64
0.8718	11.99	4.88	1.47	240.5	26.35	0.89	766.92
0.7578	9.62	6.52	0.44	240.7	27.34	1.52	766.70
0.6074	7.56	7.69	0.33	240.8	27.67	2.17	766.63
0.4250	6.10	8.40	0.32	240.8	27.88	2.73	766.59
0.2188	5.28	8.72	0.32	240.8	28.01	3.11	766.56

TABLE 7

Profiles for Catalytic Reforming in a Spherical Particle of Radius 1.6 mm

Computed with $n = 7$ and $n_w = 2$

	Concentrations, mole $cm^{-3} * 10^6$						
z	n-Heptane	Iso-heptanes	Naphthenes	Hydrogen	Toluene	Cracked Products	Temp. K
1.0000	15.84	0.	15.84	237.6	15.84	0.	769.24
0.9913	15.25	1.02	11.70	238.5	18.80	0.16	768.51
0.9540	13.00	3.74	3.41	240.3	24.83	0.80	767.01
0.8854	9.88	6.00	0.63	240.9	27.08	1.84	766.44
0.7831	6.93	7.48	0.32	240.9	27.60	3.13	766.33
0.6438	4.80	8.13	0.31	240.8	27.84	4.49	766.29
0.4641	3.55	8.15	0.30	240.7	27.97	5.73	766.28
0.2451	2.96	7.92	0.30	240.6	28.00	6.63	766.29

The naphthene and n-heptane concentrations decrease strongly toward the center of the particle, whereas the toluene, isoheptane and cracked product concentrations increase. The total intraparticle temperature drop is about 3 degrees Kelvin for both particle sizes.

CONCLUSION

A generalized model and numerical procedure have been presented here for steady-state simulation of porous catalyst particles. The examples show the ability of the method to deal with fast or slow kinetics, multicomponent diffusion and multiple reactions.

The new collocation method, with basis functions given by eqns (14), allows efficient solutions both for stiff and non-stiff differential equations. For non-stiff equations (small eigenvalues) the method reduces to a global polynomial collocation scheme. For stiff equations a similar reduction eventually occurs at large values of n, through the grouping rules described above eqns (14).

The selection of the α_j values still requires some judgment. Research on this aspect of the method is continuing.

Example 3, as well as the data in [14], show that intraparticle gradients are important in catalytic reforming operations.

Use of two pore sizes in eqn (1) is recommended for wide pore size distributions, such as commonly occur in reforming catalysts. This is more accurate than the assumption of a single pore size, and takes very little more computing time.

ACKNOWLEDGMENT

This work was supported by the National Science Foundation through Grants ENG76-24368 and CPE79-13162, by the United States Army under Contract DAAG29-80-C-0041, and by the Wisconsin Alumni Research Foundation through funds administered by the Graduate School of the

University of Wisconsin-Madison.

NOTATION

A_{kj}	weights for dimensionless gradient operator, eqn (20)
a	geometric parameter, 0 for slabs and 2 for spheres
a_{ij}	adjustable coefficients, eqn (12), consistent units
B_0	permeability coefficient, g cm sec^{-2} atm^{-1}
b_j	adjustable coefficients, eqn (17)
$\underset{\sim}{c}$	column vector with elements c_i
c	total molar concentration in pore space, mole cm^{-3}
c_i	molar concentration of species i in pore space, mole cm^{-3}
c^*	$= c_1/c_{1,0}$, dimensionless concentration of reactant species
$\underset{\sim}{D}$	matrix with elements D_{ij}
$\underset{\sim i}{D}$	row i of $\underset{\sim}{D}$
D_{ij}	transport coefficient calculated from eqns (A.2)-(A.5), consistent units
$\mathcal{D}_{ij}(c,T)$	binary diffusivity of pair ij, cm^2 sec^{-1}
$\mathcal{D}_{iK}(r)$	$= r\sqrt{32\,R\,T/9\,M_i}$, Knudsen diffusivity of gas i in a pore of radius r, cm^2 sec^{-1}
$\underset{\sim s}{D}$	surface diffusion coefficient matrix, cm^2 sec^{-1}
f_{ik}	adjustable coefficients, eqn (13), consistent units
E_{kj}	weights for dimensionless divergence operator, eqn (21)
$\underset{\sim}{F}(r)$	matrix with elements defined by eqn (2), sec cm^{-2}
$\bar{H}_i$	partial enthalpy of species i, cal $mole^{-1}$
ΔH	enthalpy of reaction, cal $mole^{-1}$
k_{eff}	effective thermal conductivity of porous medium, cal cm^{-1} sec^{-1} K^{-1}
L	half-thickness or radius of particle, cm
M_i	mass number of species i, g $mole^{-1}$

m maximum number of independent production rates R_i permitted by stoichiometry and local constraints; see discussion under eqn (10)

$\underset{\sim}{N}$ column vector with elements $\underset{\sim}{N}_1$, ... $\underset{\sim}{N}_{n_c+1}$

$\underset{\sim}{N}^{(m)}$ column vector with elements $\underset{\sim}{N}_1$, ... $\underset{\sim}{N}_{n_c}$

$\underset{\sim}{N}_i$ smoothed flux of species i, mole cm^{-2} sec^{-1}, for i = 1, ... n_c; smoothed total energy flux, cal cm^{-2} sec^{-1}, for i = E

N_{iz} z-component of $\underset{\sim}{N}_i$

N^* $= \phi^2\eta/(a+1)$, dimensionless reactant flux at z = 1

n number of interior collocation points

n_c number of gaseous species

n_w number of pore sizes in eqn (1)

p total pressure, atm

$\underset{\sim}{p}$ column vector with elements p_i

p_i partial pressure of species i in pore space, atm

Q_n leading factor in residual functions, eqn (16)

$\hat{R}_j$ specific rate of reaction j, mole g^{-1} sec^{-1}

$\underset{\sim}{R}$ column vector with elements R_i

R_i $= \rho_p \sum_j \nu_{ji} \hat{R}_j$, rate of production of species i, mole cm^{-3} sec^{-1}, for i = 1, ... n_c; $R_i = 0$ for i = E

$\langle R_i \rangle$ average of R_i over the particle volume

$\underset{\sim}{R}'$ matrix with elements $\partial R_i/\partial \xi_j$, consistent units

R gas constant, consistent units

r pore radius, A

T temperature, K

W_k porosity-tortuosity coefficient in eqn (1), dimensionless

x_i $= c_i/c$, mole fraction of species i in pore space

z dimensionless coordinate relative to L, measured from center of particle

Greek letters

α_j dimensionless parameter in basis function ϕ_j, eqn (14)

β dimensionless heat of reaction in Ref. [37]

γ dimensionless activation energy in Ref. [37]

δ_{ij} Kronecker symbol, unity when i = j and zero otherwise

η $= \langle R_1 \rangle / R_{1,0}$, effectiveness factor for single reaction

λ_k dimensionless eigenvalues of eqn (9)

μ viscosity of gas mixture, g cm^{-1} sec^{-1}

ν_{ji} stoichiometric coefficient of species i in reaction j

$\underset{\sim}{\xi}$ column vector with elements ξ_i

ξ_i $= c_i$ for $i = 1, \ldots n_c$; $\xi_i = T$ for $i = E$

ρ_p particle density, g cm^{-3}

Φ Thiele modulus

ϕ_j basis function, eqn (14)

Subscripts

E energy; element n_c+1 in column vectors $\underset{\sim}{N}$ and $\underset{\sim}{\xi}$.

H molecular hydrogen

R reference state for linearization

s auxiliary variables in Paterson-Cresswell method

z z component

0 outer surface

Superscripts

$\hat{}$ per unit mass of catalyst

$\tilde{}$ approximation in terms of basis functions; see eqns (12) and (13)

REFERENCES

[1] American Petroleum Institute Research Project 44. Selected Values of Properties of Hydrocarbons and Related Compounds, Thermodynamics Research Center, Texas A & M University, College Station, Texas.

[2] Abed R. and Rinker R. G., A.I.Ch.E. J. 1973 19 618.

[3] Aris R., The Mathematical Theory of Diffusion and Reaction in Permeable Catalysts, Vol I. Clarendon Press, Oxford, 1975.

[4] Beek J., A.I.Ch.E. J. 1961 7 337.

[5] Bird R. B., Stewart W. E. and Lightfoot E. N., Notes on Transport Phenomena, Wiley, New York, 1958.

[6] Bird R. B., Stewart W. E. and Lightfoot E. N., Transport Phenomena, Wiley, New York, 1960.

[7] Carey G. F. and Finlayson B. A. Chem. Engng Sci. 1975 30 587.

[8] Davis P. J., Interpolation and Approximation, Dover, New York, 1975.

[9] Feng C. F., Ph. D. Thesis, University of Wisconsin, Madison, Wis., 1972.

[10] Feng C. F. and Stewart W. E., Ind. Engng Chem. Fundls 1973 12 143.

[11] Feng C. F., Kostrov V. V. and Stewart W. E., Ind. Engng Chem. Fundls 1974 13 5.

[12] Finlayson B. A., The Method of Weighted Residuals and Variational Principles, Academic Press, New York, 1972.

[13] Guertin E. W., Sørensen J. P. and Stewart W. E., Comp. Chem. Engng 1977 1 197.

[14] Hettinger W. P. Jr., Keith C. D., Gring J. L. and Teter J. W., Ind. Engng Chem. 1955 47 719.

[15] Hite R. H. and Jackson R., Chem. Engng Sci. 1977 32 703.

[16] Hugo P., Chem. Engng Sci. 1965 20 975.

[17] Jackson R., Transport in Porous Catalysts, Chemical Engineering Monographs, Elsevier, New York, 1977.

[18] Kaza K. R., Villadsen J. and Jackson R., Chem. Engng Sci. 1980 35 17.

[19] Kaza K. R. and Jackson R., Chem. Engng Sci. 1980 35 1179.

[20] Kehoe J. P. G. and Aris R., Chem. Engng Sci. 1973 28 2094.

[21] Krane H. G., Groh A. B., Schulman B. L. and Sinfelt J. H., Proc. 5th World Petroleum Congress 1960 3 39.

[22] Luss D., Chem. Engng Sci. 1971 26 1713.

[23] Mason E. A., Malinauskas A. P. and Evans R. B. III, J. Chem. Phys. 1967 46 3199.

[24] Mason E. A. and Evans R. B. III, J. Chem. Educ. 1969 46 358.

[25] Mingle J. O. and Smith J. M., A.I.Ch.E. J. 1961 7 243.

[26] Paterson W. R. and Cresswell D. L., Chem. Engng Sci. 1971 26 605.

[27] Petersen E. E., Chemical Reaction Analysis, Prentice-Hall, Englewood Cliffs, N. J., 1965.

[28] Pólya G. and Szegö G., Aufgaben und Lehrsätze aus der Analysis II, Heidelberger Taschenbücher Band 74, Springer, Berlin, 1971.

[29] Sehr R. A., Chem. Engng Sci. 1958 9 145.

[30] Stewart G. W., Introduction to Matrix Computations, Academic Press, New York, 1973.

[31] Stewart W. E., Chem. Engng Sci. 1978 33 547.

[32] Stewart W. E. and Villadsen J. V., A.I.Ch.E. J. 1969 15 28.

[33] Sørensen J. P. and Stewart W. E., A.I.Ch.E. J. 1980 26 98, 104.

[34] Tee L. S., Gotoh S. and Stewart W. E., Ind. Engng Chem. Fundls 1966 5 356.

[35] Villadsen J. V. and Stewart W. E., Chem. Engng Sci. 1967 22 1483, 1968 23 1515.

[36] Villadsen J. V. and Michelsen M. L., Solution of Differential Equation Models by Polynomial Approximation, Prentice-Hall, Englewood Cliffs, N. J., 1978.

[37] Weisz P. B. and Hicks J. S., Chem. Engng Sci. 1962 17 265.

[38] Wong R. L. and Denny V. E., Chem. Engng Sci. 1975 30 709.

APPENDIX A. THE MATRIX $\underset{\sim}{D}$

Insertion of the gas-law expressions $\underset{\sim}{p} = \underset{\sim}{c}RT$ and $p = \underset{\sim}{1}^T\underset{\sim}{p}$ into eqn (1) (here $\underset{\sim}{1}^T$ is a row vector with all elements unity) gives

$$\underset{\sim}{N}^{(m)} = -\sum_{k=1}^{n_w} W_k \,[\underset{\sim}{F}(r_k)]^{-1}[\underset{\sim\sim}{\nabla}c + \underset{\sim}{c}\,\underset{\sim\sim}{\nabla}\ln T] \;-\; \underset{\sim s}{D}\,\underset{\sim\sim}{\nabla}c$$

$$-\,(B_0RT/\mu)\,[\underset{\sim}{c}\,\underset{\sim}{1}^T]\,\underset{\sim\sim}{\nabla}c \;-\; (B_0cR/\mu)\,\underset{\sim}{c}\,\underset{\sim\sim}{\nabla}T \qquad (A.1)$$

This gives the following elements of $\underset{\sim}{D}$:

For $i \neq E$ and $j \neq E$,

$$D_{ij} = -\frac{\partial \underset{\sim}{N}_i}{\partial \underset{\sim}{\nabla}c_j} = \sum_{k=1}^{n_w} W_k\,[\underset{\sim}{F}(r_k)]^{-1}_{ij} + (B_0RT/\mu)\,c_i + D_{sij} \qquad (A.2)$$

For $i \neq E$,

$$D_{iE} = -\frac{\partial \underset{\sim}{N}_i}{\partial \underset{\sim}{\nabla}T} = \sum_{k=1}^{n_w} W_k\,[\underset{\sim}{F}(r_k)^{-1}\underset{\sim}{c}]_i/T \;+\; (B_0cR/\mu)c_i \qquad (A.3)$$

The remaining elements of $\underset{\sim}{D}$ are obtained from eqns (3) and (A.2):

For $j \neq E$,

$$D_{Ej} = -\frac{\partial \underset{\sim}{N}_i}{\partial \underset{\sim}{\nabla}c_j} = \sum_{i=1}^{n_c} D_{ij}\,\bar{H}_i \qquad (A.4)$$

Finally,

$$D_{EE} = - \frac{\partial \underset{\sim}{N}_i}{\partial \underset{\sim}{\nabla} T} = \sum_{i=1}^{n_c} D_{iE} \bar{H}_i + k_{eff} \qquad (A.5)$$

The matrix $\underset{\sim}{D}(\underset{\sim}{\xi}_R)$ of eqn (9) is calculated from these expressions.

APPENDIX B. PROPERTIES OF THE GRID POINTS AND BASIS FUNCTIONS

Let $a_0, \ldots a_s$ be distinct real numbers, and let $P_0(z), \ldots P_s(z)$ be polynomials of degrees $m_0, \ldots m_s$. Then the function $\sum_i P_i(z) \exp(a_i z)$ has no more than $-1 + \sum_i (m_i + 1)$ zeros on the real axis, unless it vanishes identically; see Pólya and Szegő [28], p. 48, Theorem 75. This result can be used to bound the number of zeros of any function

$$F_M(z) = \sum_{j=0}^{M} c_j \phi_j(z) \qquad (B.1)$$

constructed from the first $M + 1$ members of the set in eqns (14).

For the slab, eqn (B.1) can be written in the form

$$F_M(z) = P_0(1-z) + P_0(1+z) + \sum_{i>0} P_i(1-z) \exp[-\alpha_i(1-z)] + \sum_{i>0} P_i(1+z) \exp[-\alpha_i(1+z)] \qquad (B.2)$$

by use of eqns (14). Here the α_i are the distinct members of the set $\{\alpha_0, \ldots \alpha_M\}$. The sum $\sum_i (m_i + 1)$ is $(m_0 + 1) + 2(m_1 + 1) + \ldots =$ $2M + 1$; hence, by the above theorem of Pólya and Szegő, the number of zeros of $F_M(z)$ on the real axis does not exceed $2M$. Since $F_M(z)$ is even, the number of zeros on the real interval $(0,\infty)$ then does not exceed M.

For the sphere, eqns (B.1) and (11) give

$$z\,F_M(z) = z\,P_0(1-z) - z\,P_0(1+z) + \sum_{i>0} P_i(1-z)\,\exp[-\alpha_i(1-z)] - \sum_{i>0} P_i(1+z)\,\exp[-\alpha_i(1+z)] \qquad (B.3)$$

The sum $\sum_i (m_i + 1)$ is now $2M + 2$; this allows, at most, $2M + 1$ real zeros for $z\,F_M(z)$, and one less for $F_M(z)$. Again, $F_M(z)$ is even and has no more than M zeros on the real interval $(0,\infty)$.

Now let ν be the number of sign changes of $Q_n(z)$ on the real interval (0,1) in a slab or sphere. The result just shown ensures that $\nu \leq n$; it also ensures that there exists an expansion $F_\nu(z)$ given by (B.1) whose sign agrees on (0,1) with that of $Q_n(z)$. Then the integral $\int_0^1 Q_n(z)\,F_\nu(z)\,z^{a-1}dz$ is nonzero, since its integrand is positive except at the zeros of $Q_n(z)$. This result is compatible with eqns (19) and (B.1) if and only if $\nu \geq n$. But $\nu \leq n$, as noted above. Hence, $\nu = n$; that is, $Q_n(z)$ has exactly n sign changes on (0,1). Each sign change is a zero, since $Q_n(z)$ is continuous.

The determinant

$$D_{M+1} = \begin{vmatrix} \phi_0(z_1) & \cdots & \phi_0(z_{M+1}) \\ \phi_1(z_1) & \cdots & \phi_1(z_{M+1}) \\ \vdots & \vdots & \vdots \\ \phi_M(z_1) & \cdots & \phi_M(z_{M+1}) \end{vmatrix} \qquad (B.4)$$

is nonzero as long as the real numbers $z_1, \ldots z_{M+1}$ are distinct and

positive, since no linear combination of $\phi_0(z)$, ... $\phi_M(z)$ can vanish at more than M distinct points on $(0,\infty)$. Therefore, the matrix $[\phi_i(z_j)]$ of eqn (22) (for which M = n) is non-singular, and the weight matrix $[A_{kj}]$ is uniquely defined. The uniqueness of $[E_{kj}]$ in eqn (23) can be proved similarly, using the basis set $\{d\phi_j(z)/dz\}$.

SECURITY CLASSIFICATION OF THIS PAGE (When Data Entered)

REPORT DOCUMENTATION PAGE		READ INSTRUCTIONS BEFORE COMPLETING FORM
1. REPORT NUMBER 2341	2. GOVT ACCESSION NO. AD-A114 580	3. RECIPIENT'S CATALOG NUMBER
4. TITLE (and Subtitle) COLLOCATION ANALYSIS OF MULTICOMPONENT DIFFUSION AND REACTIONS IN POROUS CATALYSTS		5. TYPE OF REPORT & PERIOD COVERED Summary Report - no specific reporting period 6. PERFORMING ORG. REPORT NUMBER
7. AUTHOR(s) Jan P. Sørensen and Warren E. Stewart		8. CONTRACT OR GRANT NUMBER(s) DAAG29-80-C-0041
9. PERFORMING ORGANIZATION NAME AND ADDRESS Mathematics Research Center, University of Wisconsin 610 Walnut Street Madison, Wisconsin 53706		10. PROGRAM ELEMENT, PROJECT, TASK AREA & WORK UNIT NUMBERS Work Unit Number 2 - Physical Mathematics
11. CONTROLLING OFFICE NAME AND ADDRESS U. S. Army Research Office P.O. Box 12211 Research Triangle Park, North Carolina 27709		12. REPORT DATE February 1982 13. NUMBER OF PAGES 43
14. MONITORING AGENCY NAME & ADDRESS(if different from Controlling Office)		15. SECURITY CLASS. (of this report) UNCLASSIFIED 15a. DECLASSIFICATION/DOWNGRADING SCHEDULE

16. DISTRIBUTION STATEMENT (of this Report)

Approved for public release; distribution unlimited.

17. DISTRIBUTION STATEMENT (of the abstract entered in Block 20, if different from Report)

18. SUPPLEMENTARY NOTES

19. KEY WORDS (Continue on reverse side if necessary and identify by block number)

Multicomponent Diffusion, Catalysis, Chemical Reactions, Porous Media, Collocation, Stiff Equations, Approximation with Special Functions

20. ABSTRACT (Continue on reverse side if necessary and identify by block number)

A collocation method is given for steady-state simulation of multiple reactions in porous catalysts. A realistic multicomponent diffusion model is used, which includes an allowance for pore size distribution. Hyperbolic basis functions are introduced to represent the intraparticle profiles; compact solutions are thus obtained both in the presence and absence of fast reactions. Calculations for a six-component catalytic reforming system show that the catalyst performance is strongly affected by intraparticle diffusion.

DD FORM 1 JAN 73 1473 EDITION OF 1 NOV 65 IS OBSOLETE

UNCLASSIFIED

SECURITY CLASSIFICATION OF THIS PAGE (When Data Entered)

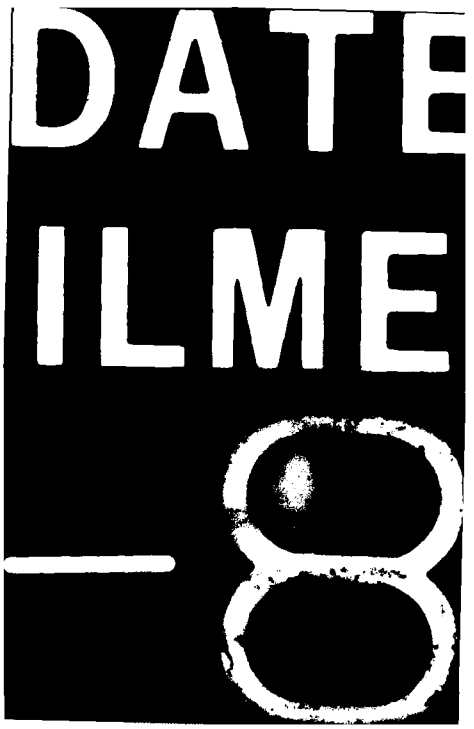
DATE
ILME
8